Supporting information: "Optimal resilience of modular interacting networks"

Dong et,al 10.1073/pnas.1922831118

Resilience represents the system's ability to retain its basic or optimal functionality in the face of various disruptions (1–9). Dynamic resilience and structural robustness are two essential aspects of overall system resilience and have attracted significant attention from the scientific community and inspired many significant studies in different areas (10–16). Several different mathematical constructs have been used to quantify various dimensions of systemic resilience. Dynamic resilience mainly focuses on a system's stability as it evolves according to single-dimension or multi-dimensional nonlinear dynamic equations. Systems encompassing a wide range of dynamical networks have been modeled through dynamic resilience, which has calculated the system response to different perturbations and helped to offer potential intervention strategies to enhance system resilience (10–13). For the case of structural robustness, researchers are typically concerned about the ability of a static topological network structure to maintain its functioning defined by connectivity, after suffering different disturbances, failures, or attacks (14–16). This framework is mainly used to analytically understand system resilience through percolation theory. This approach often also requires significant computational power to deal with large-scale networks where the theories corresponding to the thermodynamic limit can be observed.

Since the modular interacting network (MIN) system in our study is composed of large subnetworks that are coupled to each other, through specific interconnected nodes, we use percolation theory as an appropriate approach to study the resilience. The coupling patterns in the real system are diverse, not only exhibiting predetermined coupling patterns between given pairs of subnetworks, like a star, binary-tree, etc., but also including random coupling patterns where subnetworks are randomly selected to connect to some other subnetworks. To design or enhance the resilience of infrastructures, one needs to understand how resilience is affected by different coupling patterns. Here, we introduce two kinds of frameworks to study the system resilience with different deterministic coupling patterns, and random coupling pattern following some distribution.

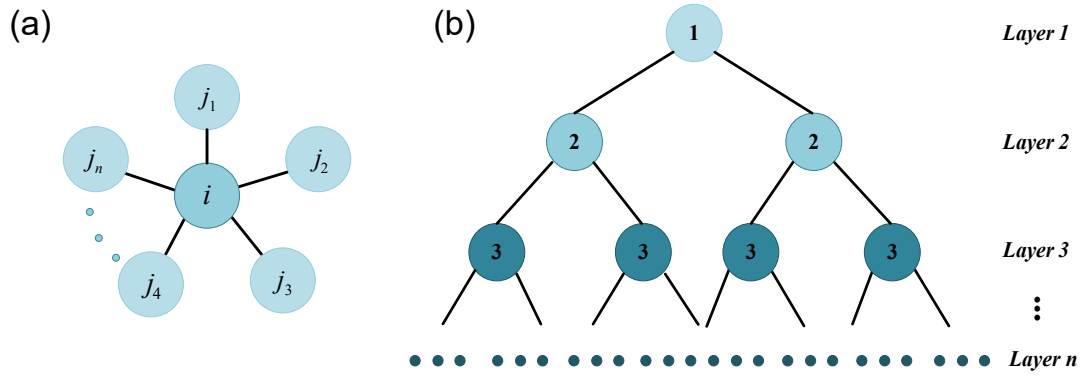

Fig. S1. Schematic representation for two types of deterministic coupling patterns. (a) Starlike coupling pattern where a central sub-network i is coupling with the other j_n subnetworks. (b) A binary tree coupling pattern where sub-network i in one layer is coupled to two subnetworks in the next layer.

Deterministic coupling pattern

For the deterministic coupling pattern, the coupling between given pairs of subnetworks is predefined, as the examples shown in Fig. S1. For this case, we define the following generating function for each sub-network i, as shown in Eq. [1] in the maintext,

$$G_i(x_{ii}, x_{ji}) = (1 - r_i) \sum_{k^i} P_s(k^i) x_{ii}^{k^i} + r_i \sum_{k^i} P_s(k^i) x_{ii}^{k^i} \prod_{j \in \Gamma_i} \sum_{k^{ji}} P_c(k^{ji}) x_{ji}^{k^{ji}}. \quad [1]$$

From Eq. [1], we can obtain the following generating functions of the branching process (14, 17),

$$\begin{cases} G_{ii}(x_{ii}, x_{ji}) = (1 - r_i) \sum_{k^i} \frac{P_s(k^i) k^i}{\langle k^i \rangle} x_{ii}^{k^i - 1} + r_i \sum_{k^i} \frac{P_s(k^i) k^i}{\langle k^i \rangle} x_{ii}^{k^i - 1} \prod_{j \in \Gamma_i} \sum_{k^{ji}} P_c(k^{ji}) x_{ji}^{k^{ji}}, \\ G_{ij}(x_{ii}, x_{ji}) = \sum_{k^i} P_s(k^i) x_{ii}^{k^i} \prod_{h \in \Gamma_i \setminus j} \sum_{k^{ji}} P_c(k^{ji}) x_{hi}^{k^{ji}} \sum_{k^{ji}} \frac{P_c(k^{ji}) k^{ji}}{\langle k^{ji} \rangle} x_{ji}^{k^{ji} - 1}, \end{cases} \quad [2]$$

where $\frac{P_s(k^i) k^i}{\langle k^i \rangle} x_{ii}^{k^i - 1}$ and $\frac{P_c(k^{ji}) k^{ji}}{\langle k^{ji} \rangle} x_{ji}^{k^{ji} - 1}$ represent probabilities of following a randomly chosen within subnetwork and between subnetwork link to a node with k^i links within subnetwork i, and k^{ji} links to subnetworks j, respectively. Here, r_i represents the fraction of nodes within subnetworks i that are also connected to the other subnetworks. And, we define $1 - f_{ii}$ and $1 - f_{ij}$

as the probability that a randomly chosen intra- and inter-link respectively, lead to a node that belong to the giant component of the system. The following self-consistent equations, Eqs. [3], can then be solved (14, 18, 19),

$$\begin{cases} f_{ii} = G_{ii}(1-p(1-f_{ii}), 1-p(1-f_{ji})), \\ f_{ji} = G_{ji}(1-p(1-f_{jj}), 1-p(1-f_{ij})). \end{cases} \quad [3]$$

We define S_i as the fraction of nodes belonging to the giant component within subnetwork i. After randomly removing $1-p$ fraction of nodes, one can obtain from Eqs. [3] and Ref. (14)

$$S_i = p\left[1 - G_i(1-p(1-f_{ii}), 1-p(1-f_{ji}))\right]. \quad [4]$$

Then the S fraction of nodes belonging to the giant component of the entire *MIN* system, can be found to be (14, 19)

$$S = \frac{\sum_i^m S_i}{m}, \quad [5]$$

where m is the number of subnetworks.

Star coupling pattern. For the case of a star coupling pattern, Fig. S1(a) shows that subnetwork i has a predetermined coupling with the other subnetworks j_h, $h = 1, \cdots, m-1$. Here, we test our theory for the case where the links within and between subnetworks follow a Poisson degree distribution. For simplicity, we let $N_i = N$, $k_i = k_{j_h} = k$, $k_{ij_h} = \bar{k}$ and $r_1 = r_{j_h} = r$, $h = 1, \cdots, m-1$. Eqs. [1]-[4] become

$$\begin{cases} G_i(x_{ii}, x_{ji}) = (1-r)e^{k(1-x_{ii})} + re^{k(1-x_{ii})}e^{(m-1)\bar{k}(1-x_{ji})}, \\ G_j(x_{jj}, x_{ij}) = (1-r)e^{k(1-x_{jj})} + re^{k(1-x_{jj})}e^{\bar{k}(1-x_{ij})}. \end{cases} \quad [6]$$

$$\begin{cases} f_{ii} = (1-r)e^{kp(f_{ii}-1))} + re^{kp(f_{ii}-1))}e^{(m-1)\bar{k}p(f_{ji}-1)}, \\ f_{ij} = e^{kp(f_{ii}-1))}e^{(m-1)\bar{k}p(f_{ji}-1)}, \\ f_{jj} = (1-r)e^{kp(f_{jj}-1))} + re^{kp(f_{jj}-1))}e^{\bar{k}p(f_{ij}-1)}, \\ f_{ji} = e^{kp(f_{jj}-1))}e^{\bar{k}p(f_{ij}-1)}. \end{cases} \quad [7]$$

$$\begin{cases} S_i = p(1-f_{ii}), \\ S_j = p(1-f_{jj}). \end{cases} \quad [8]$$

$$S = p\left[1 - \frac{1}{m}f_{ii} - \frac{m-1}{m}f_{jj}\right]. \quad [9]$$

For the special case $r = 1, k = \bar{k}$, Eq. [7] becomes

$$\begin{cases} f_{ii} = f_{ij} = e^{kp(f_{ii}-1)}e^{(m-1)kp(f_{jj}-1)}, \\ f_{jj} = f_{ji} = e^{kp(f_{jj}-1)}e^{kp(f_{ii}-1)}. \end{cases} \quad [10]$$

When the total number of links M is kept fix, the relationship between the different parameters is subject to the constraint

$$\tilde{K} = \frac{2m\mathrm{M}_{\mathrm{intra}}}{mN} + \frac{2(m-1)\mathrm{M}_{\mathrm{inter}}}{mN}, \quad [11]$$

where $\tilde{K}$ is the average of nodes in the whole MIN system, the size of subnetwork $N_i = N$, $\mathrm{M}_{\mathrm{intra}} = kN/2$ is the number of internal links in each subnetwork and $\mathrm{M}_{\mathrm{inter}} = \bar{k}rN$ is the number of inter-links between any two subnetworks. Furthermore, from Eq. [11], we can obtain

$$\tilde{K} = k + \frac{2(m-1)r\bar{k}}{m}. \quad [12]$$

As shown in Fig. S2, the theoretical results agree well with simulations for different parameter values.

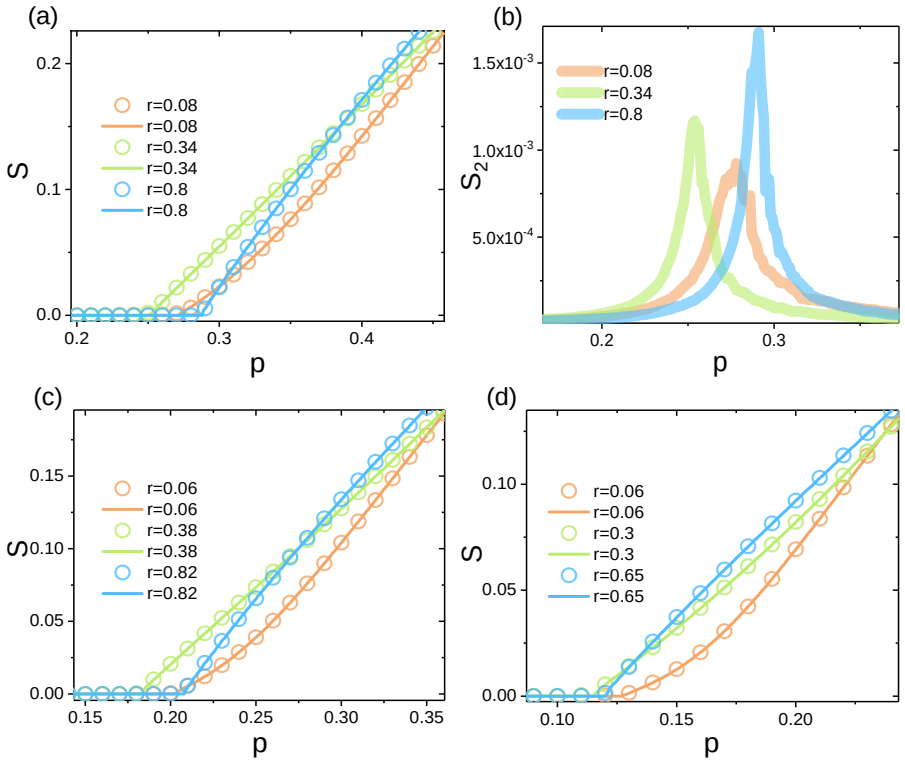

Fig. S2. Comparison between analytical (lines) and simulation (symbols) results for S as a function of p for a star coupling pattern, where the total number of links is fixed. The theory comes from Eqs. [7]-[9] and [12]. (a) The parameters are $m = 2$, $\tilde{K} = 3$ and $\bar{k} = 3$ for different values of r, (b) S_2 as a function of p with the same parameters as (a) for different r. (c) For parameters $m = 3$, $\tilde{K} = 4$ and $\bar{k} = 3$, for different values of r. (d) For $m = 4$, $\tilde{K} = 6$ and $\bar{k} = 4$, with different values of r. For the simulation results, the size of the subnetworks is $N_i = N = 10^7, i = 1, \cdots, m$ and results are averaged over 1000 independent realizations.

As $m > 2$, from Eq. [10], we get

$$p = \frac{\ln f_{jj}}{k(f_{jj}-1)+k(f_{ii}-1)} = \frac{\ln f_{jj}}{k(f_{jj}-1)+k(f_{jj}e^{(m-2)kp(f_{jj}-1)}-1)}. \quad [13]$$

For the case $r = 1$, when $f_{jj} \to 1$, the percolation threshold can be got

$$p_c = \frac{\sqrt{m-1}-1}{(m-2)k}. \quad [14]$$

Likewise, for the limit $m = 2$, $p_c = \frac{1}{2k}$ from Eq. [10], which is similar as in Ref. (14).

For the case of star coupling pattern, we consider the degree distributions within and between subnetworks follow Power-law and Poisson distributions with exponent $\lambda_i = \lambda$ and interaverage, Eqs. [1]-[4] become

$$\begin{cases} G_i(x_{ii}, x_{ji}) = (1-r)\sum_{k_i}\left[(\frac{k_i}{k_{min}+1})^{1-\lambda} - (\frac{k_i+1}{k_{min}+1})^{1-\lambda}\right] x_{ii}^{k_i} + r\sum_{k_i}\left[(\frac{k_i}{k_{min}+1})^{1-\lambda} - (\frac{k_i+1}{k_{min}+1})^{1-\lambda}\right] x_{ii}^{k_i} e^{(m-1)\bar{k}(1-x_{ji})}, \\ G_j(x_{jj}, x_{ij}) = (1-r)\sum_{k_j}\left[(\frac{k_j}{k_{min}+1})^{1-\lambda} - (\frac{k_j+1}{k_{min}+1})^{1-\lambda}\right] x_{jj}^{k_j} + r\sum_{k_j}\left[(\frac{k_j}{k_{min}+1})^{1-\lambda} - (\frac{k_j+1}{k_{min}+1})^{1-\lambda}\right] x_{jj}^{k_j} e^{\bar{k}(1-x_{ij})}. \end{cases} \quad [15]$$

$$\begin{cases} f_{ii} = & (1-r)\frac{\sum_{k_i}\left[(\frac{k_i}{k_{min}+1})^{1-\lambda} - (\frac{k_i+1}{k_{min}+1})^{1-\lambda}\right] k_i (1-p(1-f_{ii}))^{k_i-1}}{\sum_{k_i}\left[(\frac{k_i}{k_{min}+1})^{1-\lambda} - (\frac{k_i+1}{k_{min}+1})^{1-\lambda}\right] k_i} + \\ & r\frac{\sum_{k_i}\left[(\frac{k_i}{k_{min}+1})^{1-\lambda} - (\frac{k_i+1}{k_{min}+1})^{1-\lambda}\right] k_i (1-p(1-f_{ii}))^{k_i-1}}{\sum_{k_i}\left[(\frac{k_i}{k_{min}+1})^{1-\lambda} - (\frac{k_i+1}{k_{min}+1})^{1-\lambda}\right] k_i} e^{(m-1)\bar{k}p(f_{ji}-1)}, \\ f_{ij} = & \sum_{k_i}\left[(\frac{k_i}{k_{min}+1})^{1-\lambda} - (\frac{k_i+1}{k_{min}+1})^{1-\lambda}\right](1-p(1-f_{ii}))^{k_i} e^{(m-1)\bar{k}p(f_{ji}-1)}, \\ f_{jj} = & (1-r)\frac{\sum_{k_j}\left[(\frac{k_j}{k_{min}+1})^{1-\lambda} - (\frac{k_j+1}{k_{min}+1})^{1-\lambda}\right] k_j (1-p(1-f_{jj}))^{k_j-1}}{\sum_{k_j}\left[(\frac{k_j}{k_{min}+1})^{1-\lambda} - (\frac{k_j+1}{k_{min}+1})^{1-\lambda}\right] k_j} + \\ & r\frac{\sum_{k_j}\left[(\frac{k_j}{k_{min}+1})^{1-\lambda} - (\frac{k_j+1}{k_{min}+1})^{1-\lambda}\right] k_j (1-p(1-f_{jj}))^{k_j-1}}{\sum_{k_j}\left[(\frac{k_j}{k_{min}+1})^{1-\lambda} - (\frac{k_j+1}{k_{min}+1})^{1-\lambda}\right] k_j} e^{\bar{k}p(f_{ij}-1)}, \\ f_{ji} = & \sum_{k_j}\left[(\frac{k_{min}}{k_j})^{1-\lambda} - (\frac{k_{min}}{k_j+1})^{1-\lambda}\right](1-p(1-f_{jj}))^{k_j} e^{\bar{k}p(f_{ij}-1)}. \end{cases} \quad [16]$$

$$\begin{cases} S_i = p(1 - f_{ii}), \\ S_j = p(1 - f_{jj}). \end{cases} \quad [17]$$

$$S = \frac{1}{m} S_i + \frac{m-1}{m} S_j. \quad [18]$$

As Fig. S3 shows, the theoretical results agree well with simulations for different parameters.

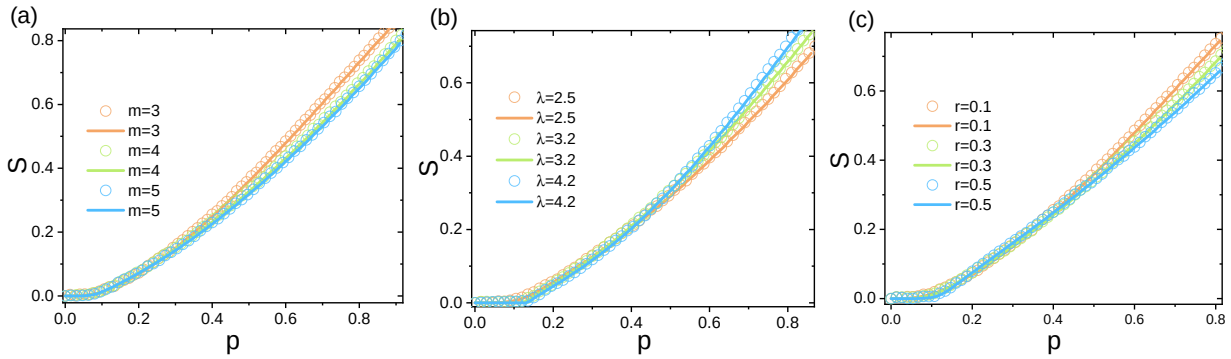

Fig. S3. Comparison between analytical (lines) and simulation (symbols) results for S as a function of p for a star coupling pattern within and between subnetworks follow Power-law and Poisson distributions. The analytical results are from Eqs. [12] and [16] - [18]. The parameters are $k_{\min} = 1$, $k_{\max} = 1000$ for the Power-law distribution. (a) $\lambda = 2.5$, $\tilde{K} = 5$, $\bar{k} = 5$ and $r = 0.3$ for different m. (b) $m = 4$, $\tilde{K} = 5$, $\bar{k} = 5$ and $r = 0.3$ for different λ. (c) $m = 3$, $\lambda = 2.5$, $\tilde{K} = 5$ and $\bar{k} = 5$ for different r. The simulation results are averaged over 1000 independent realizations for $N_i = N = 10^7, i = 1, \cdots, m$.

Binary tree coupling pattern. For the case of the binary tree coupling pattern, Fig. S1(b) shows that subnetwork i in one layer has a deterministic coupling relationship to the two subnetworks of the next layer. From Eqs. [1] - [4], we can obtain the following general formulas. For $L = 2$, Eq. [2] becomes

$$\begin{cases} G_1(x_{11}, x_{21}) = (1 - r_1) \sum_{k_1} P_s(k_1) x_{11}^{k_1} + r_1 \sum_{k_1} P_s(k_1) x_{11}^{k_1} \left[\sum_{k'} P_c(k') x_{21}^{k'} \right]^2, \\ G_2(x_{22}, x_{12}) = (1 - r_2) \sum_{k_j} P_s(k_2) x_{22}^{k_2} + r_2 \sum_{k_2} P_s(k_2) x_{22}^{k_2} \sum_{k'} P_c(k') x_{12}^{k'}, \end{cases} \quad [19]$$

and for $L > 2$, Eq. [2] becomes

$$\begin{cases} G_1(x_{11}, x_{21}) = (1 - r_1) \sum_{k_1} P_s(k_1) x_{11}^{k_1} + r_1 \sum_{k_1} P_s(k_1) x_{11}^{k_1} \left[\sum_{k'} P_c(k') x_{21}^{k'} \right]^2, \\ G_2(x_{22}, x_{12}, x_{32}) = (1 - r_2) \sum_{k_j} P_s(k_2) x_{22}^{k_2} + r_2 \sum_{k_2} P_s(k_2) x_{22}^{k_2} \sum_{k'} P_c(k') x_{12}^{k'} \left[\sum_{k'} P_c(k') x_{32}^{k'} \right]^2, \\ \cdots \\ G_{L-1}(x_{L-1,L-1}, x_{L-2,L-1}, x_{L,L-1}) = (1 - r_{L-1}) \sum_{k_j} P_s(k_{L-1}) x_{L-1,L-1}^{k_{L-1}} + \\ r_{L-1} \sum_{k_{L-1}} P_s(k_{L-1}) x_{L-1,L-1}^{k_{L-1}} \sum_{k'} P_c(k') x_{L-2,L-1}^{k'} \left[\sum_{k'} P_c(k') x_{L,L-1}^{k'} \right]^2, \\ G_L(x_{L,L}, x_{L-1,L}) = (1 - r_L) \sum_{k_j} P_s(k_L) x_{L,L}^{k_L} + r_L \sum_{k_L} P_s(k_L) x_{L,L}^{k_L} \sum_{k'} P_c(k') x_{L-1,L}^{k'}. \end{cases} \quad [20]$$

For both cases, Eqs. [3] - [5] become

$$\begin{cases} f_{ii} = G_{ii}(1 - p(1 - f_{ii}), 1 - p(1 - f_{ji})), \\ f_{ji} = G_{ji}(1 - p(1 - f_{jj}), 1 - p(1 - f_{ij})). \end{cases} \quad [21]$$

$$S_i = p\left[1 - G_i(1 - p(1 - f_{ii}), 1 - p(1 - f_{ji}))\right], \quad [22]$$

and

$$S = \frac{\sum_{l=1}^{L} 2^{l-1} S_i}{2^L - 1}. \quad [23]$$

Additionally, when the number of total links is kept fix, the relations between the different parameters will be

$$\begin{cases} \tilde{K} = \frac{2\mathrm{M}_{\mathrm{intra}}(2^{\mathrm{L}}-1) + 2\mathrm{M}_{\mathrm{inter}} 2(2^{\mathrm{L}-1}-1)}{(2^L-1)N}, \\ \mathrm{M}_{\mathrm{intra}} = \frac{kN}{2}, \\ \mathrm{M}_{\mathrm{inter}} = \frac{2krN}{2}. \end{cases} \quad [24]$$

Simplifying these gives,

$$\tilde{K} = k + \frac{4r\bar{k}(2^{L-1}-1)}{2^L - 1}. \quad [25]$$

We apply our theory for the case where the degree distributions within and between subnetworks follow Poisson distributions. For simplify let $k_i = k$, $k_{ij} = \bar{k}$, $r_i = r$ and $N_i = N$. As $L = 2$, Eq. [21] becomes

$$\begin{cases} f_{11} = (1-r)e^{kp(f_{11}-1)} + re^{kp(f_{11}-1)}e^{2\bar{k}p(f_{21}-1)}, \\ f_{12} = e^{kp(f_{11}-1)}e^{2\bar{k}p(f_{21}-1)}, \\ f_{22} = (1-r)e^{kp(f_{22}-1)} + re^{kp(f_{22}-1)}e^{\bar{k}p(f_{12}-1)}, \\ f_{21} = e^{kp(f_{22}-1)}e^{\bar{k}p(f_{12}-1)}, \end{cases} \quad [26]$$

As $L > 2$, Eqs. [21] - [23] become

$$\begin{cases} f_{11} = (1-r)e^{kp(f_{11}-1)} + re^{kp(f_{11}-1)}e^{2\bar{k}p(f_{21}-1)}, \\ f_{12} = e^{kp(f_{11}-1)}e^{2\bar{k}p(f_{21}-1)}, \\ f_{22} = (1-r)e^{kp(f_{22}-1)} + re^{kp(f_{22}-1)}e^{\bar{k}p(f_{12}-1)}e^{2\bar{k}p(f_{32}-1)}, \\ f_{21} = f_{23} = e^{kp(f_{22}-1)}e^{\bar{k}p(f_{12}-1)}e^{2\bar{k}p(f_{32}-1)}, \\ \ldots \\ f_{L,L} = (1-r)e^{kp(f_{L,L}-1)} + re^{kp(f_{L,L}-1)}e^{\bar{k}p(f_{L-1,L}-1)}, \\ f_{L,L-1} = e^{kp(f_{L,L}-1)}e^{\bar{k}p(f_{L-1,L}-1)}. \end{cases} \quad [27]$$

$$\begin{cases} S_i = p(1-f_{ii}), \\ S = p(1 - \frac{\sum_{l=1}^{L} 2^{l-1} f_{l,l}}{2^L - 1}). \end{cases} \quad [28]$$

Fig. S4(a) shows that the analytical and simulation results agree well. One can observe that the system exhibits an optimal r^* for different parameter sets when the total number of links remain unchanged from Fig. S4(c)-(e). The critical threshold p_c in these figures is determined by the peak values of the second-largest component S_2, as shown in Fig. S4(b).

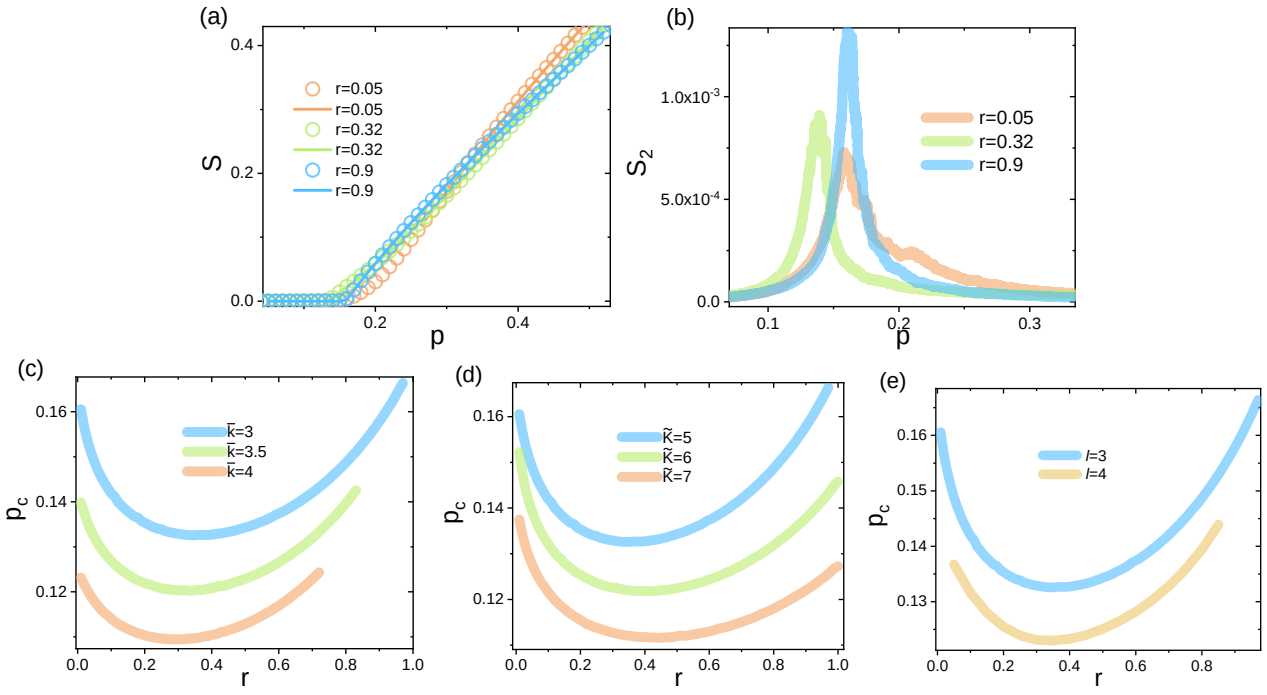

Fig. S4. (a) Comparison between analytical (lines) and simulation (symbols) results for a binary tree coupling pattern with Poisson degree distributions within and between subnetworks. S as a function of p is shown, and the analytical results are obtained from Eqs. [25], [27] and [28]. The parameters here are $L = 3$, $\tilde{K} = 5$, $\bar{k} = 3$. (b) S_2 as a function of p for different r with the same parameters as (a). (c)-(e) p_c as a function of r are from Eqs. [27] and [28] for different parameters (c) $L = 3$ and $\tilde{K} = 5$, (d) $L = 3$ and $\bar{k} = 3$, and (e) $\tilde{K} = 5$ and $\bar{k} = 3$. Simulation results are averaged over 1000 independent realizations with $N_i = N = 10^7$.

For the binary tree coupling pattern, the degree within and between subnetworks follow power-law distribution with exponent $\lambda_i = \lambda$ and Poisson distribution with interaverage degree $\bar{k}$. As $L = 2$, Eq. [21] becomes

$$\begin{cases} f_{11} = (1-r)\frac{\sum_{k_1}\left[(\frac{k_1}{k_{min}+1})^{1-\lambda}-(\frac{k_1+1}{k_{min}+1})^{1-\lambda}\right]k_1(1-p(1-f_{11}))^{k_1-1}}{\sum_{k_1}\left[(\frac{k_1}{k_{min}+1})^{1-\lambda}-(\frac{k_1+1}{k_{min}+1})^{1-\lambda}\right]k_1}+ \\ r\frac{\sum_{k_1}\left[(\frac{k_1}{k_{min}+1})^{1-\lambda}-(\frac{k_1+1}{k_{min}+1})^{1-\lambda}\right]k_1(1-p(1-f_{11}))^{k_1-1}}{\sum_{k_1}\left[(\frac{k_1}{k_{min}+1})^{1-\lambda}-(\frac{k_1+1}{k_{min}+1})^{1-\lambda}\right]k_1}e^{2\bar{k}p(f_{21}-1)}, \\ f_{12} = \sum_{k_1}\left[(\frac{k_1}{k_{min}+1})^{1-\lambda}-(\frac{k_1+1}{k_{min}+1})^{1-\lambda}\right](1-p(1-f_{11}))^{k_1}e^{2\bar{k}p(f_{21}-1)}, \\ f_{22} = (1-r)\frac{\sum_{k_2}\left[(\frac{k_2}{k_{min}+1})^{1-\lambda}-(\frac{k_2+1}{k_{min}+1})^{1-\lambda}\right]k_2(1-p(1-f_{22}))^{k_2-1}}{\sum_{k_2}\left[(\frac{k_2}{k_{min}+1})^{1-\lambda}-(\frac{k_2+1}{k_{min}+1})^{1-\lambda}\right]k_2}+ \\ r\frac{\sum_{k_2}\left[(\frac{k_2}{k_{min}+1})^{1-\lambda}-(\frac{k_2+1}{k_{min}+1})^{1-\lambda}\right]k_2(1-p(1-f_{22}))^{k_2-1}}{\sum_{k_2}\left[(\frac{k_2}{k_{min}+1})^{1-\lambda}-(\frac{k_2+1}{k_{min}+1})^{1-\lambda}\right]k_2}e^{\bar{k}p(f_{12}-1)}, \\ f_{21} = \sum_{k_2}\left[(\frac{k_{min}}{k_2})^{1-\lambda}-(\frac{k_{min}}{k_2+1})^{1-\lambda}\right](1-p(1-f_{22}))^{k_2}e^{\bar{k}p(f_{12}-1)}. \end{cases} \quad [29]$$

For $L > 2$, Eqs. [21]-[23] become

$$\begin{cases} f_{11} = (1-r)\frac{\sum_{k_1}\left[(\frac{k_1}{k_{min}+1})^{1-\lambda}-(\frac{k_1+1}{k_{min}+1})^{1-\lambda}\right]k_1(1-p(1-f_{11}))^{k_1-1}}{\sum_{k_1}\left[(\frac{k_1}{k_{min}+1})^{1-\lambda}-(\frac{k_1+1}{k_{min}+1})^{1-\lambda}\right]k_1}+ \\ r\frac{\sum_{k_1}\left[(\frac{k_1}{k_{min}+1})^{1-\lambda}-(\frac{k_1+1}{k_{min}+1})^{1-\lambda}\right]k_1(1-p(1-f_{11}))^{k_1-1}}{\sum_{k_1}\left[(\frac{k_1}{k_{min}+1})^{1-\lambda}-(\frac{k_1+1}{k_{min}+1})^{1-\lambda}\right]k_1}e^{2\bar{k}p(f_{21}-1)}, \\ f_{12} = \sum_{k_1}\left[(\frac{k_1}{k_{min}+1})^{1-\lambda}-(\frac{k_1+1}{k_{min}+1})^{1-\lambda}\right](1-p(1-f_{11}))^{k_1}e^{2\bar{k}p(f_{21}-1)}, \\ f_{22} = (1-r)\frac{\sum_{k_2}\left[(\frac{k_2}{k_{min}+1})^{1-\lambda}-(\frac{k_2+1}{k_{min}+1})^{1-\lambda}\right]k_2(1-p(1-f_{22}))^{k_2-1}}{\sum_{k_2}\left[(\frac{k_2}{k_{min}+1})^{1-\lambda}-(\frac{k_2+1}{k_{min}+1})^{1-\lambda}\right]k_2}+ \\ r\frac{\sum_{k_2}\left[(\frac{k_2}{k_{min}+1})^{1-\lambda}-(\frac{k_2+1}{k_{min}+1})^{1-\lambda}\right]k_2(1-p(1-f_{22}))^{k_2-1}}{\sum_{k_2}\left[(\frac{k_2}{k_{min}+1})^{1-\lambda}-(\frac{k_2+1}{k_{min}+1})^{1-\lambda}\right]k_2}e^{2\bar{k}p(f_{12}-1)}e^{\bar{k}p(f_{32}-1)}, \\ f_{21} = f_{23} = \sum_{k_2}\left[(\frac{k_{min}}{k_2})^{1-\lambda}-(\frac{k_{min}}{k_2+1})^{1-\lambda}\right](1-p(1-f_{22}))^{k_2}e^{2\bar{k}p(f_{12}-1)}e^{\bar{k}p(f_{32}-1)}, \\ \cdots \\ f_{L,L} = (1-r)\frac{\sum_{k_L}\left[(\frac{k_L}{k_{min}+1})^{1-\lambda}-(\frac{k_L+1}{k_{min}+1})^{1-\lambda}\right]k_L(1-p(1-f_{L,L}))^{k_L-1}}{\sum_{k_L}\left[(\frac{k_L}{k_{min}+1})^{1-\lambda}-(\frac{k_L+1}{k_{min}+1})^{1-\lambda}\right]k_L}+ \\ r\frac{\sum_{k_L}\left[(\frac{k_L}{k_{min}+1})^{1-\lambda}-(\frac{k_L+1}{k_{min}+1})^{1-\lambda}\right]k_L(1-p(1-f_{L,L}))^{k_L-1}}{\sum_{k_L}\left[(\frac{k_L}{k_{min}+1})^{1-\lambda}-(\frac{k_L+1}{k_{min}+1})^{1-\lambda}\right]k_L}e^{\bar{k}p(f_{L-1,L}-1)}, \\ f_{L,L-1} = \sum_{k_L}\left[(\frac{k_{min}}{k_L})^{1-\lambda}-(\frac{k_{min}}{k_L+1})^{1-\lambda}\right](1-p(1-f_{L,L}))^{k_L}e^{\bar{k}p(f_{L-1,L}-1)}. \end{cases} \quad [30]$$

$$S_i = p\left[1 - G_i(1-p(1-f_{ii}), 1-p(1-f_{ji}))\right]. \quad [31]$$

$$S = \frac{\sum_{l=1}^{L} 2^{L-1} S_i}{2^L - 1} \quad [32]$$

The theoretical results are testified by simulation results, as shown in Fig. S5.

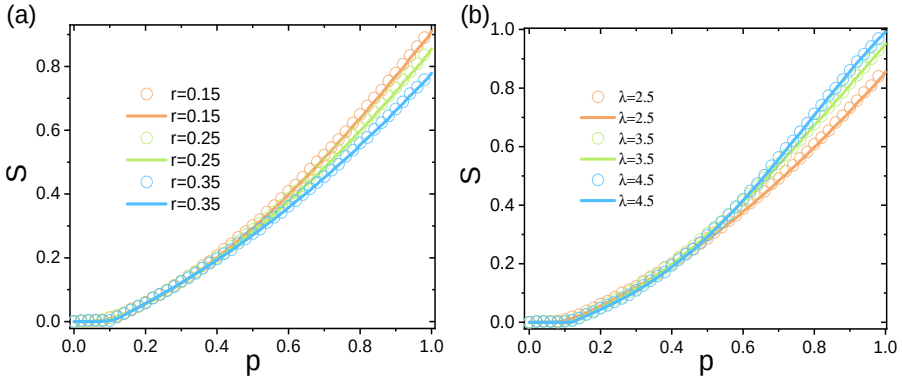

Fig. S5. Comparison between analytical (lines) and simulation (symbols) results for S as a function of p. Analytical results are from Eqs. [30]-[32]. (a) The parameters are $L = 3$, $\lambda = 2.5$, $\bar{K} = 4$, and $\bar{k} = 4$. (b) The parameters are $L = 3$, $\bar{K} = 4$, $\bar{k} = 4$, and $r = 0.25$. Simulation results are averaged over 1000 independent realizations with $N_i = N = 10^7$.

Besides the above examples, one can use the above analytical approach and generating functions to investigate the structural resilience of any system with specific predetermined coupling patterns.

Random coupling pattern

In this section, we focus on coupling patterns based on random coupling following different distributions like random regular (RR), Poisson, and power-law distributions (see Fig. 1 in the main text). The generating function for subnetwork i is shown in Eq. [1] of the main paper. The following branching generating functions are (14, 17),

$$\begin{cases} G_{ii}(x_{ii},x_{ji}) = (1-r_i)\sum_{k_i}\frac{P_s(k_i)k_i}{\langle k_i\rangle}x_{ii}^{k_i-1} + r_i\sum_{k_i}\frac{P_s(k_i)k_i}{\langle k_i\rangle}x_{ii}^{k_i-1}\sum_K P_u(K)\left[\sum_{k^{ji}}P_c(k^{ji})x_{ji}^{k^{ji}}\right]^K, \\ G_{ij}(x_{ii},x_{ji}) = \sum_{k_i}P_s(k_i)x_{ii}^{k_i}\sum_K\frac{P_u(K)K}{\langle K\rangle}\left[\sum_{k^{ji}}P_c(k^{ji})x_{ji}^{k^{ji}}\right]^{K-1}\sum_{k^{ji}}\frac{P_c(k^{ji})k^{ji}}{\langle k^{ji}\rangle}x_{ji}^{k^{ji}-1}. \end{cases} \quad [33]$$

where $\frac{P_u(K)K}{\langle K\rangle}\left[\sum_{k^{ji}}P_c(k^{ji})x_{ji}^{k^{ji}}\right]^{K-1}$ represents the probability of following a randomly chosen link to a subnetwork from a subnetwork with K links in the MIN system. Similar to Eqs. [3] and [4], $1-f_{ii}$ and $1-f_{ij}$, represent the probabilities that a randomly chosen link within or between subnetworks belongs to the giant component respectively are

$$\begin{cases} f_{ii} = G_{ii}(1-p(1-f_{ii}),1-p(1-f_{ji})), \\ f_{ji} = G_{ji}(1-p(1-f_{jj}),1-p(1-f_{ij})). \end{cases} \quad [34]$$

For the case of random coupling pattern, a node locating in the giant component of MIN must belong to the giant cluster S_i of subnetwork i, and also that the giant cluster S_i should be contained in the largest component $\bar{S}$ of the overall MIN. Thus,

$$S = \bar{S}\cdot S_i. \quad [35]$$

The largest component $\bar{S}$ composed of subnetworks connected via a random coupling pattern can be described by (17)

$$\bar{S} = 1-\bar{G}_0(X) = 1-\sum_K P_u(K)X^K. \quad [36]$$

After randomly removing $1-p$ fraction of nodes, one can obtain from Eqs. [34] and Ref. (14),

$$S_i = p\left[1-G_i(1-p(1-f_{ii}),1-p(1-f_{ji}))\right]. \quad [37]$$

RR coupling pattern. For the RR coupling pattern with average degree K, where $P_u(K)=1$ and for all inputs other than K the probability is zero. Then, Eq. [1] in the main paper becomes,

$$G_i(x_{ii},x_{ji}) = (1-r_i)\sum_{k^i}P_s(k^i)x_{ii}^{k^i} + r_i\sum_{k^i}P_s(k^i)x_{ii}^{k^i}[\sum_{k^{ji}}P_c(k^{ji})x_{ji}^{k^{ji}}]^K. \quad [38]$$

For the case of nodes within and between the subnetworks both following Poisson degree distributions, we assume $N_i=N$, $k_i=k$, $k_{ij}=\bar{k}$ and $r_i=r$, $i,j=1,\cdots,m$, Eqs. [34]-[37] become

$$\begin{cases} f_{ii} = (1-r)e^{kp(f_{ii}-1)} + re^{kp(f_{ii}-1)+K\bar{k}p(f_{ji}-1)}, \\ f_{ji} = e^{kp(f_{ii}-1)+K\bar{k}p(f_{ji}-1)}, \end{cases} \quad [39]$$

$$\begin{cases} S_i = p[1-G_i(1-p(1-f_{ii}),1-p(1-f_{ji}))], \\ S = p(1-f_{ii}). \end{cases} \quad [40]$$

From Eq. [39], we can obtain

$$p = \frac{\ln f_{ji}}{k(f_{ii}-1)+K\bar{k}(f_{ji}-1)} = \frac{\ln\frac{f_{ii}-(1-r)e^{kp(f_{ii}-1)}}{r}}{k(f_{ii}-1)+K\bar{k}(\frac{f_{ii}-(1-r)e^{kp(f_{ii}-1)}}{r}-1)}. \quad [41]$$

In the limit $f_{jj}\to 1$, one can obtain the critical threshold

$$p_c = \frac{(k+\bar{k}K)-\sqrt{(k-\bar{k}K)^2+4k\bar{k}Kr}}{2k\bar{k}K(1-r)}. \quad [42]$$

Similarly, for keeping the total number of links fixed, we get

$$\tilde{K} = \frac{2(\mathrm{M_{intra}}+K\mathrm{M_{inter}})}{N} = k+r\bar{k}K. \quad [43]$$

Fig. S6(a)-(b) shows comparison of analytical and simulation results. It can be seen that simulation results agree well with the analytical predictions. In Fig. S6(c), S_2 as a function of p is shown, and p_c being determined by the location of peak value of S_2 .

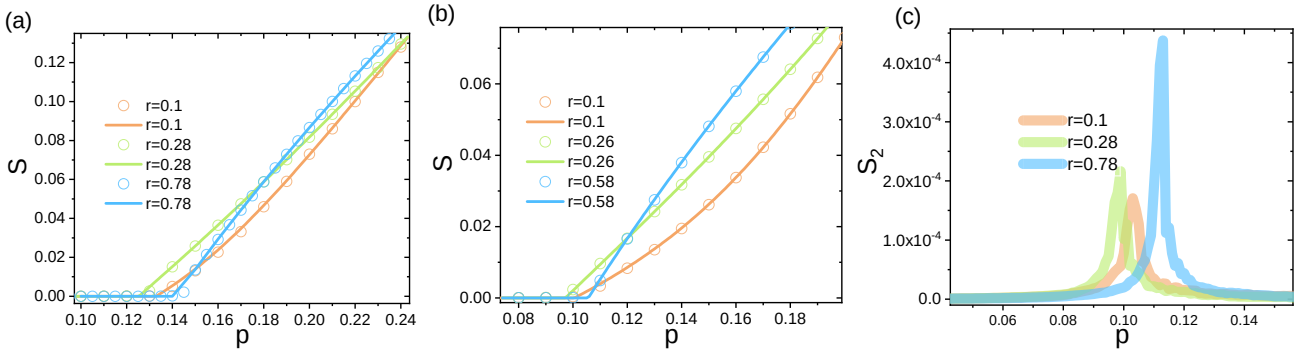

Fig. S6. Comparison between analytical (lines) and simulation (symbols) results of S as a function of p for a RR coupling pattern. Analytical results are from Eqs. [39], [40] and [43] for different r. (a) The parameters are $\tilde{K}=6$, $K=2$ and $\bar{k}=3$ for different r. (b) $\tilde{K}=6$, $K=3$ and $\bar{k}=3$ for different r. (c) S_2 as a function of p with the same parameters as (b) for different r. Simulation results are averaged over 1000 independent realizations with $N_i=N=10^6$ and $m=10^4$.

We next consider for the case of nodes within and between the subnetworks both following Power-law and Poisson degree distributions. For simplify, let $N_i=N$, $\lambda_i=\lambda$, $k_{ij}=\bar{k}$ and $r_i=r$, $i,j=1,\cdots,m$. Eqs. [34]-[37] become

$$\begin{cases} f_{ii}=(1-r)\dfrac{\sum_{k_i}\left[(\frac{k_i}{k_{\min}+1})^{1-\lambda}-(\frac{k_i+1}{k_{\min}+1})^{1-\lambda}\right]k_i(1-p(1-f_{ii}))^{k_i-1}}{\sum_{k_i}\left[(\frac{k_i}{k_{\min}+1})^{1-\lambda}-(\frac{k_i+1}{k_{\min}+1})^{1-\lambda}\right]k_i}+ \\ r\dfrac{\sum_{k_i}\left[(\frac{k_i}{k_{\min}+1})^{1-\lambda}-(\frac{k_i+1}{k_{\min}+1})^{1-\lambda}\right]k_i(1-p(1-f_{ii}))^{k_i-1}}{\sum_{k_i}\left[(\frac{k_i}{k_{\min}+1})^{1-\lambda}-(\frac{k_i+1}{k_{\min}+1})^{1-\lambda}\right]k_i}e^{K\bar{k}p(f_{ji}-1)}, \\ f_{ji}=\sum_{k_i}\left[(\frac{k_i}{k_{\min}+1})^{1-\lambda}-(\frac{k_i+1}{k_{\min}+1})^{1-\lambda}\right](1-p(1-f_{ii}))^{k_i}e^{K\bar{k}p(f_{ji}-1)}, \end{cases} \quad [44]$$

where $k_{\min}$ denotes the minimum degree within subnetwork. We then have

$$\begin{cases} S_i=p\left[1-G_i(1-p(1-f_{ii}),1-p(1-f_{ji}))\right], \\ S=S_i. \end{cases} \quad [45]$$

In Fig. S7, we observe that analytical results agree well with simulation results.

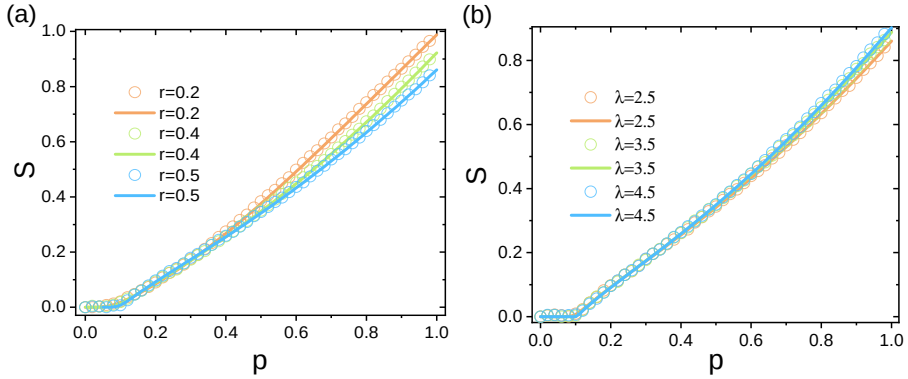

Fig. S7. Comparison between analytical (lines) and simulation (symbols) results for S as a function of p. Analytical results are from Eqs. [44] and [45] with parameters $k_{\min}=1$ and $k_{\max}=1000$. (a) The parameters are $\tilde{K}=6$, $K=3$, $\bar{k}=3$ and $\lambda=2.5$ for different r. (b)$\tilde{K}=6$, $K=3$, $\bar{k}=3$ and $r=0.5$ for different λ. Simulation results are averaged over 1000 independent realizations with $N_i=N=10^6$ and $m=10^4$.

Poisson coupling pattern. In this subsection, we study the Poisson coupling pattern, and assume that each subnetwork is connected to average K other subnetworks. For the case of nodes within and between the subnetworks both following Poisson degree distributions with average degrees $k_i=k$, $k_{ij}=\bar{k}$, let $N_i=N$, $r_i=r$, $i,j=1,\cdots,m$, Eqs. [34]-[36] become

$$\begin{cases} f_{ii}=(1-r)e^{kp(f_{ii}-1)}+re^{kp(f_{ii}-1)}e^{K(e^{\bar{k}p(f_{ji}-1)}-1)}, \\ f_{ji}=e^{kp(f_{ii}-1)}e^{K(e^{\bar{k}p(f_{ji}-1)}-1)}e^{\bar{k}p(f_{ji}-1)}. \end{cases} \quad [46]$$

$$\begin{cases} S_i = p\left[1 - G_i(1 - p(1 - f_{ii}), 1 - p(1 - f_{ji}))\right], \\ \bar{S} = 1 - e^{-K\bar{S}}, \\ S = \bar{S} \cdot S_i. \end{cases} \quad [47]$$

In the limit $r = 1, k\bar{k} \neq 0$, from Eq. [46], we find

$$p = \frac{\ln f_{ii} - K(e^{\bar{k}p(f_{ji}-1)} - 1)}{k(f_{ii} - 1)} = \frac{\ln \frac{f_{ji}}{e^{\bar{k}p(f_{ji}-1)}} - K(e^{\bar{k}p(f_{ji}-1)} - 1)}{k(\frac{f_{ji}}{e^{\bar{k}p(f_{ji}-1)}} - 1)}. \quad [48]$$

Furthermore, as $f_{ji} \to 1$, we obtain

$$p_c = \frac{(k + \bar{k} + \bar{k}K) - \sqrt{(k + \bar{k} + \bar{k}K)^2 - 4k\bar{k}}}{2k\bar{k}}. \quad [49]$$

In a different limit of $r = 1$ and $k = 0$, from Eq. [46], we get

$$p = \frac{\ln f_{ji} - K(e^{\bar{k}p(f_{ji}-1)} - 1)}{\bar{k}(f_{ji} - 1)}. \quad [50]$$

Similarly, for $f_{ji} \to 1$,

$$p_c = \frac{1}{\bar{k}(K + 1)}. \quad [51]$$

For this case, the same formula as Eq. [43] can be used for the case where the number of links is held fixed. We see in Fig. S8 that analytical results agree well with simulation results.

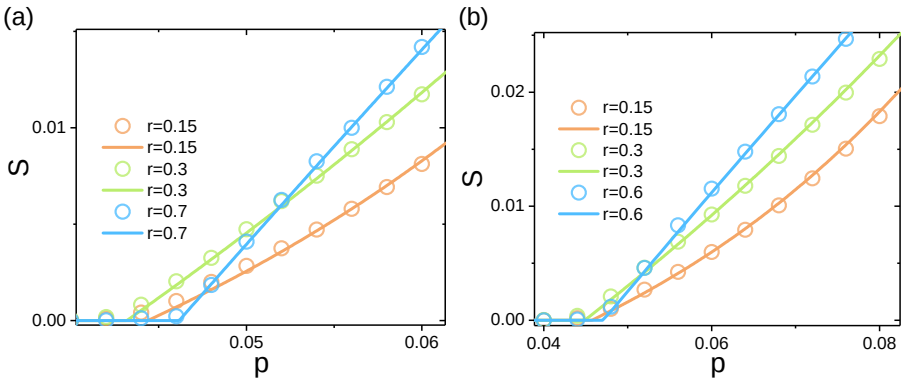

Fig. S8. Comparison between analytical (lines) and simulation (symbols) results for S as a function of p for a Poisson coupling pattern. Analytical results are from Eqs. [46] and [47]. (a) The parameters are $\bar{K} = 14$, $K = 4$, $\bar{k} = 4$ for different r (b) $\bar{K} = 12$, $K = 4$ and $\bar{k} = 4$ for different r. Simulation results are averaged over 1000 independent realizations with $N_i = N = 10^6$ and $m = 10^4$.

For the case of nodes within and between the subnetworks both following Power-law with exponent $\lambda_i = \lambda$ and Poisson degree distributions with same average degree $\bar{k}$, Eqs. [34]-[36] become

$$\begin{cases} f_{ii} = (1 - r)\frac{\sum_{k_i}\left[(\frac{k_i}{k_{\min}+1})^{1-\lambda} - (\frac{k_i+1}{k_{\min}+1})^{1-\lambda}\right]k_i(1-p(1-f_{ii}))^{k_i-1}}{\sum_{k_i}\left[(\frac{k_i}{k_{\min}+1})^{1-\lambda} - (\frac{k_i+1}{k_{\min}+1})^{1-\lambda}\right]k_i} + \\ r\frac{\sum_{k_i}\left[(\frac{k_i}{k_{\min}+1})^{1-\lambda} - (\frac{k_i+1}{k_{\min}+1})^{1-\lambda}\right]k_i(1-p(1-f_{ii}))^{k_i-1}}{\sum_{k_i}\left[(\frac{k_i}{k_{\min}+1})^{1-\lambda} - (\frac{k_i+1}{k_{\min}+1})^{1-\lambda}\right]k_i} e^{K(e^{\bar{k}p(f_{ji}-1)}-1)}, \\ f_{ji} = \sum_{k_i}\left[(\frac{k_i}{k_{\min}+1})^{1-\lambda} - (\frac{k_i+1}{k_{\min}+1})^{1-\lambda}\right](1 - p(1 - f_{ii}))^{k_i} e^{K(e^{\bar{k}p(f_{ji}-1)}-1)} e^{\bar{k}p(f_{ji}-1)}. \end{cases} \quad [52]$$

$$\begin{cases} S_i = p\left[1 - G_i(1 - p(1 - f_{ii}), 1 - p(1 - f_{ji}))\right], \\ \bar{S} = 1 - e^{-K\bar{S}}, \\ S = \bar{S} \cdot S_i. \end{cases} \quad [53]$$

Fig. S9 shows the agreement between analytical and simulation results for different parameters.

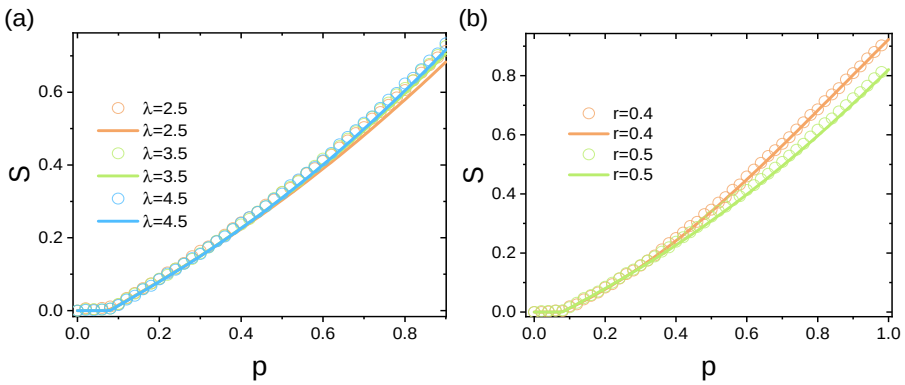

Fig. S9. Comparison between analytical (lines) and simulation (symbols) results for S as a function of p for a Poisson coupling pattern. Analytical results are from Eqs. (52) and (53) with parameters $k_{\min} = 1$ and $k_{\max} = 1000$. (a) Here $\bar{K} = 6$, $K = 3$, $\bar{k} = 3$ and $r = 0.5$ for varying λ, (b) Here $\bar{K} = 6$, $K = 3$, $\bar{k} = 3$ and $\lambda = 3.5$ for different r. Simulation results are averaged over 1000 independent realizations with $N_i = N = 10^6$ and $m = 10^4$.

Power-law coupling pattern. Here we consider the Power-law coupling pattern where each subnetwork connects to a number of other subnetworks follows a power-law degree distribution with exponent λ, average degree K and minimum degree $k_{\min}$. We first deal with the case where the degree within and between the subnetworks follow Poisson distribution with average degrees k and $\bar{k}$. We assume $r_i = r, i = 1, \cdots, m$, Eqs. [34]-[36] become

$$\begin{cases} f_{ii} = (1-r)e^{kp(f_{ii}-1)} + re^{kp(f_{ii}-1)} \sum_K \left[(\frac{K}{k_{\min}+1})^{1-\lambda} - (\frac{K+1}{k_{\min}+1})^{1-\lambda} \right] e^{K\bar{k}p(f_{ji}-1)}, \\ f_{ji} = e^{kp(f_{ii}-1)} \frac{\sum_K \left[(\frac{K}{k_{\min}+1})^{1-\lambda} - (\frac{K+1}{k_{\min}+1})^{1-\lambda} \right] K e^{(K-1)\bar{k}p(f_{ji}-1)}}{\sum_K \left[(\frac{K}{k_{\min}+1})^{1-\lambda} - (\frac{K+1}{k_{\min}+1})^{1-\lambda} \right] K} e^{\bar{k}p(f_{ji}-1)}, \end{cases} \quad [54]$$

$$\begin{cases} \bar{G}_0(X) = \sum_K \left[(\frac{K}{k_{\min}+1})^{1-\lambda} - (\frac{K+1}{k_{min}+1})^{1-\lambda} \right] X^K, \\ \bar{S} = 1 - \bar{G}_0(\bar{f}), \end{cases} \quad [55]$$

$$\begin{cases} S_i = p\left[1 - G_i(1 - p(1-f_{ii}), 1 - p(1-f_{ji}))\right], \\ S = \bar{S} \cdot S_i. \end{cases} \quad [56]$$

Fig. S10 shows comparison between analytical and simulation results for the different parameters.

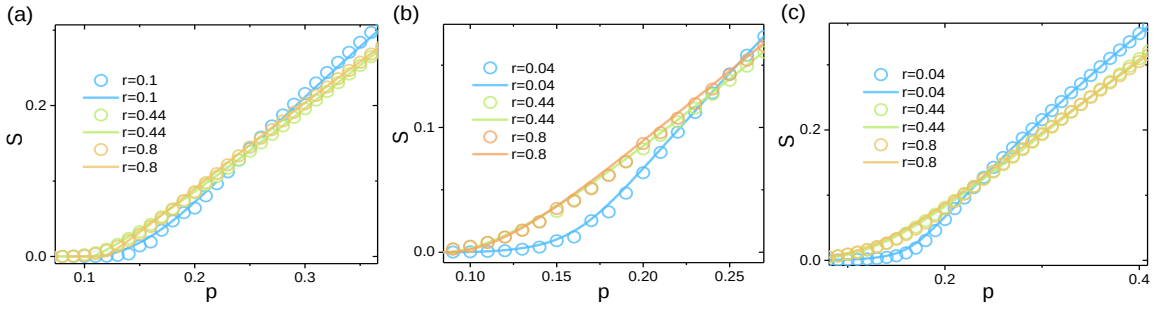

Fig. S10. Comparison between analytical (lines) and simulation (symbols) results of S as a function of p for a power-law coupling pattern. Analytic results are from Eqs. (54)-(56) with parameters $k_{\min} = 2$ and $k_{\max} = 1000$. (a) The remaining parameters here are $\lambda = 4.5$, $\bar{k} = 2.5$ and $K = 2$. (b) Here we show results for $\lambda = 3.5$, $\bar{k} = 2.5$ and $K = 2$ with varying r. (c) Here we show results for $\lambda = 2.5$, $\bar{k} = 2.5$ and $K = 2$ for varying r. Simulation results are averaged over 100 independent realizations with $N_i = N = 10^5$ and $m = 10^5$.

We next consider a power-law coupling pattern with exponent λ, minimum degree $K_{\min}$ and the maximum degree $K_{\max}$. For the case of nodes within and between the subnetworks both following Power-law degree distributions with exponent $\lambda_i = \bar{\lambda}$, average degree k, minimum degree $k_{\min}$, maximum degree $k_{\max}$, and $\lambda_{ij} = \lambda^{'}$, minimum degree $\bar{k}_{\min}$, maximum degree $\bar{k}_{\max}$,

we assume $K_{\min}=\bar{k}_{\min}=k_{\min}$ and $K_{\max}=\bar{k}_{\max}=k_{\max}$. Then, Eqs. [34]-[36] become

$$\begin{cases} f_{ii}=(1-r)\dfrac{\sum_{k_i}\left[(\frac{k_i}{k_{\min}+1})^{1-\tilde{\lambda}}-(\frac{k_i+1}{k_{\min}+1})^{1-\tilde{\lambda}}\right]k_i(1-p(1-f_{ii}))^{k_i-1}}{\sum_{k_i}\left[(\frac{k_i}{k_{\min}+1})^{1-\tilde{\lambda}}-(\frac{k_i+1}{k_{\min}+1})^{1-\tilde{\lambda}}\right]k_i}+ \\ r\dfrac{\sum_{k_i}\left[(\frac{k_i}{k_{\min}+1})^{1-\tilde{\lambda}}-(\frac{k_i+1}{k_{\min}+1})^{1-\tilde{\lambda}}\right]k_i(1-p(1-f_{ii}))^{k_i-1}}{\sum_{k_i}\left[(\frac{k_i}{k_{\min}+1})^{1-\tilde{\lambda}}-(\frac{k_i+1}{k_{\min}+1})^{1-\tilde{\lambda}}\right]k_i} \\ \sum_K\left[(\frac{K}{k_{\min}+1})^{1-\lambda}-(\frac{K+1}{k_{\min}+1})^{1-\lambda}\right]\left[\sum_{k'}\left[(\frac{k\prime}{k_{\min}+1})^{1-\lambda'}-(\frac{k'+1}{k_{min}+1})^{1-\lambda'}\right](1-p(1-f_{ji}))^{k'}\right]^K, \\ f_{ji}=\sum_{k_i}\left[(\frac{k_i}{k_{\min}+1})^{1-\tilde{\lambda}}-(\frac{k_i+1}{k_{\min}+1})^{1-\tilde{\lambda}}\right](1-p(1-f_{ii}))^{k_i} \\ \dfrac{\sum_K\left[(\frac{K}{k_{\min}+1})^{1-\lambda}-(\frac{K+1}{k_{\min}+1})^{1-\lambda}\right]K\left[\sum_{k'}\left[(\frac{k\prime}{k_{\min}+1})^{1-\lambda'}-(\frac{k'+1}{k_{min}+1})^{1-\lambda'}\right](1-p(1-f_{ji}))^{k'}\right]^{K-1}}{\sum_K\left[(\frac{K}{k_{\min}+1})^{1-\lambda}-(\frac{K+1}{k_{\min}+1})^{1-\lambda}\right]K} \\ \dfrac{\sum_{k'}\left[(\frac{k\prime}{k_{\min}+1})^{1-\lambda'}-(\frac{k'+1}{k_{\min}+1})^{1-\lambda'}\right]k'(1-p(1-f_{ji}))^{k'-1}}{\sum_{k'}\left[(\frac{k\prime}{k_{\min}+1})^{1-\lambda'}-(\frac{k'+1}{k_{\min}+1})^{1-\lambda'}\right]k'}. \end{cases} \quad [57]$$

$$\begin{cases} \bar{G}_0(X)=\sum_K\left[(\frac{K}{k_{\min}+1})^{1-\lambda}-(\frac{K+1}{k_{\min}+1})^{1-\lambda}\right]X^K, \\ \bar{S}=1-\bar{G}_0(\bar{f}), \end{cases} \quad [58]$$

$$\begin{cases} S_i=p\left[1-G_i(1-p(1-f_{ii}),1-p(1-f_{ji}))\right], \\ S=\bar{S}\cdot S_i. \end{cases} \quad [59]$$

As shown in Fig. S11, one can see that analytical results agree well with simulation results.

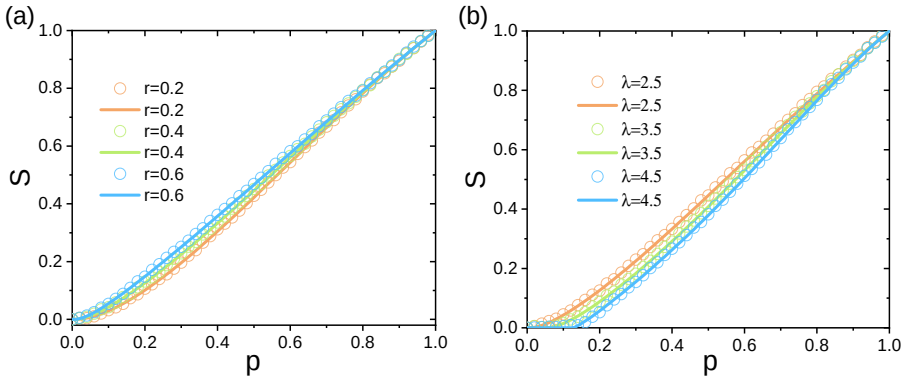

Fig. S11. Comparison between analytical (lines) and simulation (symbols) results for S as a function of p for a power-law coupling pattern with power-law degree distributions within and between subnetworks. The analytical results are from Eqs. (57)-(59) with parameters $k_{\min}=2$ and $k_{\max}=1000$. (a) The parameters here are $\tilde{\lambda}=2.5$, $\lambda'=2.5$ and $\lambda=2.5$ with different r. (b) $r=0.3$ for different $\tilde{\lambda}=\lambda'=\lambda$. Simulation results are averaged over 500 independent realizations with $N_i=N=10^5$ and $m=10^5$.

M&A network Data

From analyzing M&A network data of 18 years (2001-2018), the general information and statistical features for the two largest M&A regions, Asia and America, are shown in Table S1,

	Asia	America	Inter Network
Node	28165	19672	5269
Link	32037	21706	4588
Average Degree	2.274951	2.206791	1.741501
Min Degree	0	0	1
Max Degree	544	253	211
λ	2.6	2.6	2.6
r	0.12117877	0.09205978	

Table S1. General information and statistical features.

The degree within subnetwork for Asia and America regions show Power-law distributions as shown in Fig. S12.

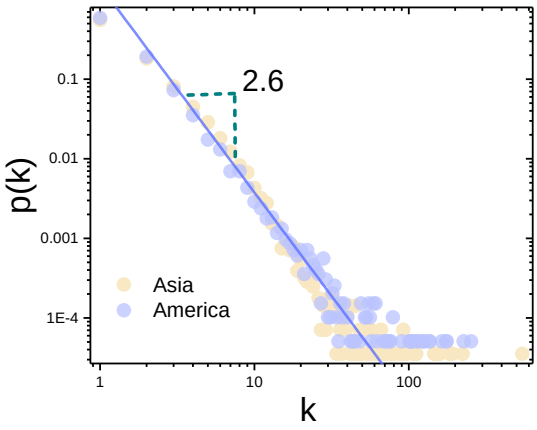

Fig. S12. The degree distribution of two subnetworks.

Fig. S13(a)-(c) show comparison of simulation results between the network model and the real network for S as a function of p. One can notice that there exists an optimal r^* which is the same as the real network, as shown in Fig. 5(b) of the main paper. Here the threshold p_c is determined by using of peak value of S_2.

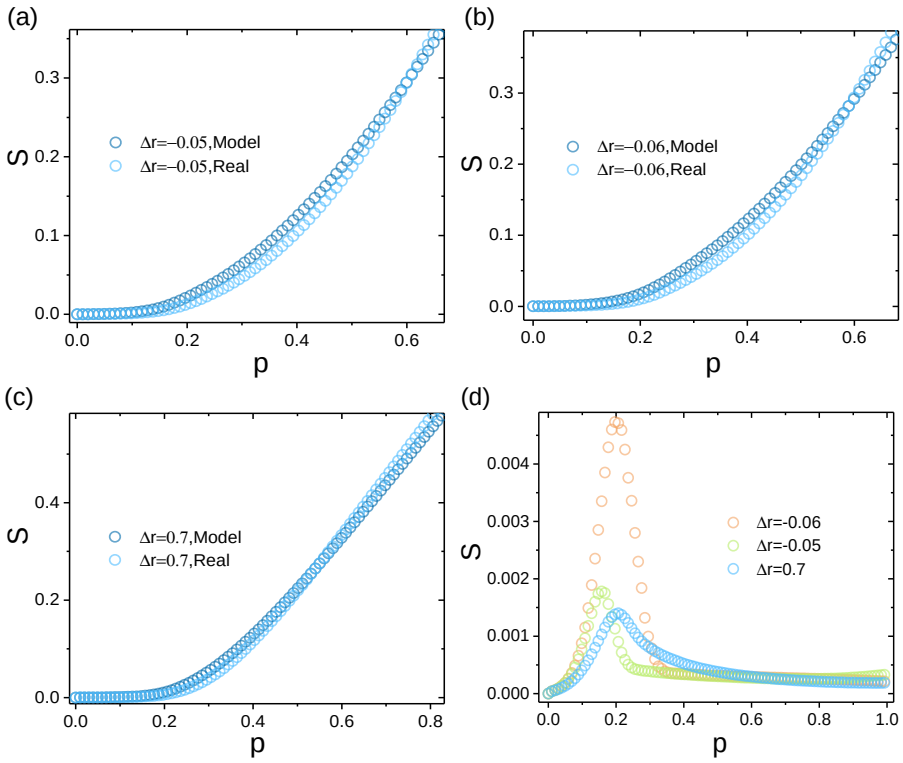

Fig. S13. (a)-(c) Comparison of simulation results for S as a function of p for network model and real network with the same parameters, as shown in Table S1, for different Δr. (d) S_2 as a function of p for different Δr for real network.

1. Cohen R, Erez K, Ben-Avraham D, Havlin S (2000) Resilience of the internet to random breakdowns. *Physical Review Letters* 85(21):4626.
2. Dorogovtsev SN, Goltsev AV, Mendes JF (2008) Critical phenomena in complex networks. *Reviews of Modern Physics* 80(4):1275.
3. Radicchi F, Castellano C (2015) Breaking of the site-bond percolation universality in networks. *Nature Communications* 6(1):1–7.
4. Cohen R, Ben-Avraham D, Havlin S (2002) Percolation critical exponents in scale-free networks. *Physical Review E* 66(3):036113.
5. Schneider CM, Moreira AA, Andrade JS, Havlin S, Herrmann HJ (2011) Mitigation of malicious attacks on networks. *Proceedings of the National Academy of Sciences of the United States of America* 108(10):3838–3841.
6. Tanizawa T, Paul G, Cohen R, Havlin S, Stanley HE (2005) Optimization of network robustness to waves of targeted and random attacks. *Physical Review E* 71(4):047101.
7. Eriksen KA, Simonsen I, Maslov S, Sneppen K (2003) Modularity and extreme edges of the internet. *Physical Review Letters* 90(14):148701.
8. Achlioptas D, D'Souza RM, Spencer J (2009) Explosive percolation in random networks. *Science* 323(5920):1453–1455.
9. Girvan M, Newman ME (2002) Community structure in social and biological networks. *Proceedings of the national academy of sciences of the United States of America* 99(12):7821–7826.
10. Allesina S, Tang S (2012) Stability criteria for complex ecosystems. *Nature* 483(7388):205–208.
11. Gao J, Barzel B, Barabási AL (2016) Universal resilience patterns in complex networks. *Nature* 530(7590):307–312.
12. Rohr RP, Saavedra S, Bascompte J (2014) On the structural stability of mutualistic systems. *Science* 345(6195).
13. Duan D, et al. (2019) Universal behavior of cascading failures in interdependent networks. *Proceedings of the National Academy of Sciences of the United States of America* 116(45):22452–22457.

14. Dong G, et al. (2018) Resilience of networks with community structure behaves as if under an external field. *Proceedings of the National Academy of Sciences of the United States of America* 115(27):6911–6915.
15. Wu J, Barahona M, Tan Yj, Deng Hz (2012) Robustness of random graphs based on graph spectra. *Chaos: An Interdisciplinary Journal of Nonlinear Science* 22(4):043101.
16. Morone F, Makse HA (2015) Influence maximization in complex networks through optimal percolation. *Nature* 524(7563):65–68.
17. Newman ME, Strogatz SH, Watts DJ (2001) Random graphs with arbitrary degree distributions and their applications. *Physical Review E* 64(2):026118.
18. Shao S, Huang X, Stanley HE, Havlin S (2015) Percolation of localized attack on complex networks. *New Journal of Physics* 17(2):023049.
19. Shai S, et al. (2015) Critical tipping point distinguishing two types of transitions in modular network structures. *Physical Review E* 92(6):062805.